PNAS RESEARCH ARTICLE | MEDICAL SCIENCES

Lysophosphatidic acid triggers inflammation in the liver and white adipose tissue in rat models of 1-acyl-sn-glycerol-3-phosphate acyltransferase 2 deficiency and overnutrition

Ikki Sakuma[a,b], Rafael C. Gaspar[a], Panu K. Luukkonen[a], Mario Kahn[a], Dongyan Zhang[a], Xuchen Zhang[c], Sue Murray[d], Jaya Prakash Golla[a], Daniel F. Vatner[a], Varman T. Samuel[a], Kitt Falk Petersen[a], and Gerald I. Shulman[a,e,f,1]

Contributed by Gerald I. Shulman; received July 27, 2023; accepted November 10, 2023; reviewed by Rebecca j. Brown and Elif A. Oral

AGPAT2 (1-acyl-sn-glycerol-3-phosphate-acyltransferase-2) converts lysophosphatidic acid (LPA) into phosphatidic acid (PA), and mutations of the *AGPAT2* gene cause the most common form of congenital generalized lipodystrophy which leads to steatohepatitis. The underlying mechanism by which AGPAT2 deficiency leads to lipodystrophy and steatohepatitis has not been elucidated. We addressed this question using an antisense oligonucleotide (ASO) to knockdown expression of *Agpat2* in the liver and white adipose tissue (WAT) of adult male Sprague-Dawley rats. *Agpat2* ASO treatment induced lipodystrophy and inflammation in WAT and the liver, which was associated with increased LPA content in both tissues, whereas PA content was unchanged. We found that a controlled-release mitochondrial protonophore (CRMP) prevented LPA accumulation and inflammation in WAT whereas an ASO against *glycerol-3-phosphate acyltransferase, mitochondrial* (*Gpam*) prevented LPA content and inflammation in the liver in *Agpat2* ASO-treated rats. In addition, we show that overnutrition, due to high sucrose feeding, resulted in increased hepatic LPA content and increased activated macrophage content which were both abrogated with *Gpam* ASO treatment. Taken together, these data identify LPA as a key mediator of liver and WAT inflammation and lipodystrophy due to AGPAT2 deficiency as well as liver inflammation due to overnutrition and identify LPA as a potential therapeutic target to ameliorate these conditions.

congenital generalized lipodystrophy | lysophosphatidic acid | inflammation | phosphatidic acid | AGPAT2

Significance

Mutations of the *AGPAT2* (1-acyl-sn-glycerol-3-phosphate-acyltransferase-2) gene cause congenital generalized lipodystrophy and hepatic inflammation through unknown mechanisms. Knockdown of *Agpat2* expression in liver and white adipose tissue (WAT), using an antisense oligonucleotide (ASO), leads to increased LPA content and inflammation in these tissues. A controlled-release mitochondrial protonophore prevented LPA accumulation and inflammation in WAT, whereas knockdown of *mitochondrial glycerol-3-phosphate acyltransferase (Gpam)* with an ASO prevented LPA accumulation and inflammation in liver. Overnutrition due to high sucrose feeding also increased LPA content and activated macrophages in the liver, which were both abrogated with knockdown of hepatic Gpam expression. These data demonstrate that LPA is a trigger of liver and WAT inflammation due to AGPAT2 deficiency and overnutrition.

The enzyme, 1-acyl-sn-glycerol-3-phosphate acyltransferase 2 (AGPAT2), catalyzes an intermediate step in triglyceride biosynthesis converting lysophosphatidic acid (LPA) into phosphatidic acid (PA) by incorporating an acyl moiety at the *sn*-2 position of the glycerol backbone (1). AGPAT2 is expressed predominantly in adipose tissue and the liver, and mutations of the *AGPAT2* gene are responsible for the most common form of congenital generalized lipodystrophy Type 1 (CGL1), which can lead to insulin resistance, hypertriglyceridemia, and steatohepatitis (2).

Consistent with human CGL1, *Agpat2* knockout mice develop severe lipodystrophy, adipose tissue inflammation, and hepatic steatosis (3, 4). Newborn *Agpat2* knouckout mice are born with near-normal adipose tissue depots, which are lost during the first week of life (4). AGPAT2-deficient adipocytes would be predicted to have an impaired capacity to adapt to the massive lipid availability associated with postnatal feeding, leading to cellular stress, death, and inflammatory destruction of adipose tissue (4).

Hepatic steatosis has been attributed to activation of an alternative monoacylglycerol pathway for triglyceride biosynthesis as well as spillover of excess triglyceride to the liver. Hepatic de novo lipogenesis is activated in the *Agpat2* knockout mouse (3). However, the mechanism by which AGPAT2 deficiency leads to lipodystrophy, adipose tissue inflammation, and steatohepatitis has not been sufficiently elucidated (3–9).

LPA is a bioactive lipid that belongs to the class of lysophospholipids, phospholipids with a single fatty acyl chain (10). LPA can trigger inflammation through G-protein coupled receptors (LPAR1-6), which exhibit widespread tissue distribution (11). LPA mediates proinflammatory responses via macrophage activation in intestinal inflammation, psoriasis, and multiple sclerosis (12–14). Given that LPA is a substrate of AGPAT2, we hypothesized that AGPAT2 deficiency raises LPA tissue content in an inappropriate, unregulated fashion, triggering inflammation in the liver and white adipose tissue (WAT) and promoting involution of WAT. We tested this hypothesis using an antisense oligonucleotide (ASO) to knock down the expression of *Agpat2* in the liver and WAT of adult male Sprague-Dawley (SD) rats and assessed its impact on liver and WAT inflammation and tissue LPA content. In addition, we also examined the potential role for LPA in

[1]To whom correspondence may be addressed. Email: gerald.shulman@yale.edu.

This article contains supporting information online at https://www.pnas.org/lookup/suppl/doi:10.1073/pnas.2312666120/-/DCSupplemental.

Published December 21, 2023.

mediating liver inflammation in a rat model of high-sucrose feeding overnutrition.

Results

***Agpat2* ASO Suppresses AGPAT2 Expression and Increases LPA in the Liver and WAT.** Four weeks of *Agpat2* ASO treatment in regular chow-fed male SD rats decreased AGPAT2 protein expression by 60% in the liver and 40% in WAT (Fig. 1 *A*–*C*). While actual body weights did not show significant change at each time point between *Agpat2* ASO-treated rats and control ASO-treated rats (*SI Appendix*, Fig. S1), the body weight ratio of each time point/basal time point before ASO injection was lower in *Agpat2* ASO-treated rats compared to control ASO-treated rats, potentially due to loss of WAT (Fig. 1*D*). Knockdown of *Agpat2* resulted in a 1.8-fold and 1.9-fold increase in LPA in the *Agpat2*

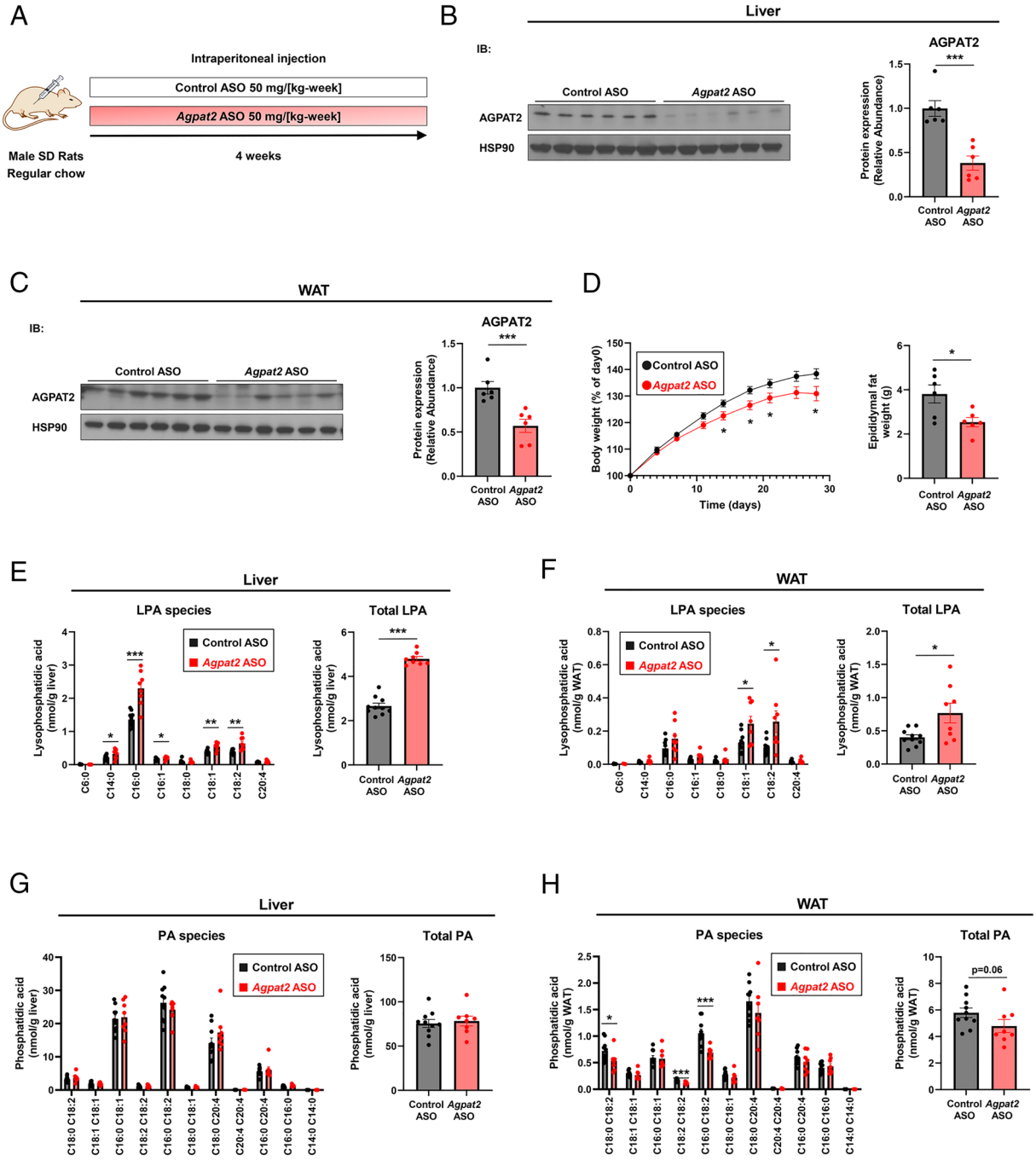

Fig. 1. *Agpat2* ASO suppresses AGPAT2 expression and increases LPA in the liver and WAT. (*A*) Male SD rats were fed regular chow and treated with 50 mg/kg/week *Agpat2* ASO or control ASO for four weeks. (*B* and *C*) AGPAT2 protein expression was analyzed in the liver (*B*) and WAT (*C*) by immunoblot analysis. *Agpat2* ASO decreased AGPAT2 protein expression in the liver and WAT. (*D*) The *Left* panel shows the body weight ratio of each time point/basal time point before ASO injection in ad libitum regular chow-fed rats (control ASO $n = 10$, *Agpat2* ASO $n = 8$). *$P < 0.05$ compared with control ASO-treated rats within each time point by the Student *t* test. The right panel shows weight of epididymal fat (control ASO $n = 6$, *Agpat2* ASO $n = 6$). (*E*–*H*) LPA and PA were extracted from livers and WATs and measured by tandem mass spectrometry (control ASO $n = 10$, *Agpat2* ASO $n = 8$). (*E*) Total hepatic LPA content was increased in *Agpat2* ASO-treated rats. Most abundant LPA species in the liver was palmitoyl LPA (C16:0). (*F*) The total WAT LPA content was increased in *Agpat2* ASO-treated rats. Oleoyl LPA (C18:1) and linoleic LPA (C18:2) showed relatively high concentrations among the LPA species in WAT. (*G*) Total hepatic PA content, as well as all individual PA species, showed no differences. (*H*) Total WAT PA concentrations slightly decreased in *Agpat2* ASO-treated rats. Three species decreased significantly: C18:0/C18:2, C18:2/C18:2, and C16:0/C18:2. The data are shown as the mean ± SEM. *$P < 0.05$; **$P < 0.01$; and ***$P < 0.001$ (Student *t* test).

ASO-treated rat liver and WAT, respectively (Fig. 1 *E* and *F*). While the most abundant LPA species in the liver was LPA (C16:0), LPA (C18:1) and LPA (C18:2) showed relatively high levels among the LPA species in WAT. Although PA is the product of AGPAT2, total hepatic PA content and all individual PA species showed no differences (Fig. 1*G*). Total WAT PA concentrations, which could be attributed to specific PA species (C18:0/C18:2, C18:2/C18:2, and C16:0/C18:2), were slightly reduced in *Agpat2* ASO-treated rats (Fig. 1*H*).

***Agpat2* ASO Induces Inflammation in the Liver and WAT and Leads to Loss of WAT.** *Agpat2* ASO treatment increased hepatic macrophage infiltration assessed by H-E staining as well as an increase in CD68-positive cells (Fig. 2 *A* and *B*). While hepatic triglyceride content was not different between the two groups (Fig. 2*C*), the expression of the macrophage marker *F4/80* and inflammatory marker *TNFα* mRNA were both significantly increased (Fig. 2*D*) and plasma AST concentration was also slightly increased in *Agpat2* ASO-treated rats compared to control ASO-treated rats (Fig. 2*E*).

Agpat2 ASO treatment increased WAT macrophage infiltration as determined by increased CD68-positive cells (Fig. 2 *F* and *G*). Additionally, crown-like structures, composed of macrophages surrounding dead or dying adipocytes, increased dramatically in *Agpat2* ASO-treated rats compared to control ASO-treated rats (Fig. 2*F*). Consistent with these results, RT-qPCR revealed that macrophage marker *F4/80* mRNA expression significantly increased in *Agpat2* ASO-treated rats compared to control ASO-treated rats (Fig. 2*H*). A previous *Agpat2* knockout mice study demonstrated that lipodystrophy results from postnatal cell death of adipose tissue in association with inflammation (4). We therefore evaluated cell death in WAT of *Agpat2* ASO-treated rats by terminal deoxynucleotidyl transferase dUTP nick end labeling (TUNEL) staining. TUNEL-positive cells were undetectable in WAT of control ASO-treated rats. In contrast, TUNEL-positive cells were abundant in the *Agpat2* ASO-treated rats (Fig. 2*F*). The distribution of adipocyte size shifted toward a smaller size in *Agpat2* ASO-treated rats compared to control ASO-treated rats (Fig. 2*I*). Accordingly, RT-qPCR showed that adipocyte marker adiponectin *(Adipoq)* mRNA expression significantly decreased in *Agpat2* ASO-treated rats compared to control ASO-treated rats (Fig. 2*H*). The expression of adipocyte marker proteins (ATGL and HSL) was also much lower in *Agpat2* ASO-treated rats compared to control ASO-treated rats (Fig. 2*J*). ATGL and HSL regulate WAT lipolysis, and consistent with lower expression of ATGL and HSL in WAT, fasting plasma NEFA concentrations were significantly lower in *Agpat2* ASO-treated rats than in the control ASO-treated rats (Fig. 2*K*), whereas plasma insulin concentrations were similar in the two groups.

LPA Induces *TNFα* Expression in Immortalized Mouse Kupffer Cells and Suppresses Adipocyte Differentiation in 3T3-L1 Cells. LPA has previously been shown to regulate macrophage activation and inhibit adipocyte differentiation in vitro (12, 15, 16). To determine whether LPA in and of itself could promote hepatic inflammation, we investigated the effects of LPA on NF-kB (p65) protein phosphorylation and the mRNA expression of *TNFα* using Immortalized Mouse Kupffer Cells (ImKC) (Fig. 3 *A*–*C*). Palmitoyl LPA (C16:0) or oleoyl LPA (C18:1) treatment increased NF-kB (p65) phosphorylation. *TNFα* mRNA expression also increased following palmitoyl LPA (C16:0) or oleoyl LPA (C18:1) treatment.

To test the putative antiadipogenic activity of LPA, we evaluated the effect of LPA on mRNA expression of adipogenic transcription factor *Pparg* and downstream adipogenic markers (*Adipoq, Fabp4, and Lpl*) using the 3T3-L1 preadipocyte differentiation model (Fig. 3 *D* and *E*). Gene expression of *Pparg*, *Adipoq, Fabp4, and Lpl* decreased in palmitoyl LPA (C16:0)-treated, and oleoyl LPA (C18:1)-treated 3T3-L1 cells compared to differentiated control (Fig. 3*E*).

Controlled-release Mitochondrial Protonophore Treatment Prevents LPA Accumulation and Inflammation in WAT in AGPAT2 Deficiency. We previously reported that controlled-release mitochondrial protonophore (CRMP) reverses nonalcoholic steatohepatitis in lipodystrophic AZIP/F-1 mice (17). To determine whether CRMP might also be effective in preventing AGPAT2 deficiency-induced adipose/liver inflammation and LPA accumulation, we studied *Agpat2* ASO-treated rats with or without CRMP for 4 wk, followed by measurement of inflammatory markers and LPA and PA tissue content in the liver and WAT (Fig. 4*A*). CRMP treatment had divergent effects on hepatic lipid metabolism. CRMP did not alter total hepatic LPA content (Fig. 4*B*) or hepatic PA content (Fig. 4*C*). Though CRMP-treatment reduced hepatic triglycerides content by 50% (Fig. 4*F*) it did not alter liver inflammation, as reflected by H-E staining of the liver and RT-qPCR markers of inflammation (Fig. 4 *G* and *H*). In contrast, CRMP treatment reduced total LPA content in WAT (Fig. 4*D*), which could mostly be attributed to reductions in LPA (C16:0), LPA(C16:1), LPA (C18:0), LPA (C18:1), and LPA (C18:2) (Fig. 4*D*). CRMP treatment had no effect on total PA content or on individual PA species in WAT (Fig. 4*E*). CRMP-treatment suppressed AGPAT2 deficiency-induced macrophage infiltration and the number of CD68-positive cells in WAT (Fig. 4 *I* and *J*). Additionally, crown-like structures decreased in CRMP-treated rats compared to the controls (Fig. 4*J*). Consistent with these results, RT-qPCR showed that CRMP treatment significantly decreased *F4/80* mRNA expression compared to control rats (Fig. 4*K*). The distribution of adipocyte size shifted toward a larger size in CRMP-treated rats compared to the controls (Fig. 4*L*). Accordingly, RT-qPCR showed that the adipocyte marker adiponectin mRNA expression significantly increased in CRMP-treated rats compared to the controls (Fig. 4*K*). The protein expression of ATGL and HSL was also increased in CRMP-treated rats compared to control rats (Fig. 4*M*). Consistent with these findings, plasma NEFA concentrations in CRMP-treated rats were also slightly higher than in control rats (Fig. 4*N*) while plasma insulin concentrations showed a strong tendency to be decreased in CRMP-treated rats compared to the control animals independent of any changes in plasma glucose concentrations.

***Glycerol-3-phosphate Acyltransferase, Mitochondrial* ASO Prevents Hepatic LPA Accumulation and Inflammation in AGPAT2 Deficiency.** We previously reported that glycerol-3-phosphate acyltransferase, mitochondrial (GPAM) knockout mice demonstrated decreased hepatic LPA content (18). GPAM converts glycerol-3-phosphate into LPA, the upstream reaction of AGPAT2, and therefore contributes to the synthesis of triglyceride, particularly in the liver (19). To examine whether *Gpam* ASO might be effective in decreasing AGPAT2 deficiency-induced liver inflammation and LPA accumulation, we studied *Agpat2* ASO-treated rats that were also treated with either a *Gpam* ASO or control ASO for four weeks, followed by evaluation of liver and adipose metabolites and inflammation markers (Fig. 5*A*). The total hepatic LPA content was decreased in *Gpam* ASO-treated rats. LPA(C16:0), LPA(C16:1), LPA (C18:1), and LPA (C18:2) were primarily decreased (Fig. 5*B*), whereas total hepatic PA content

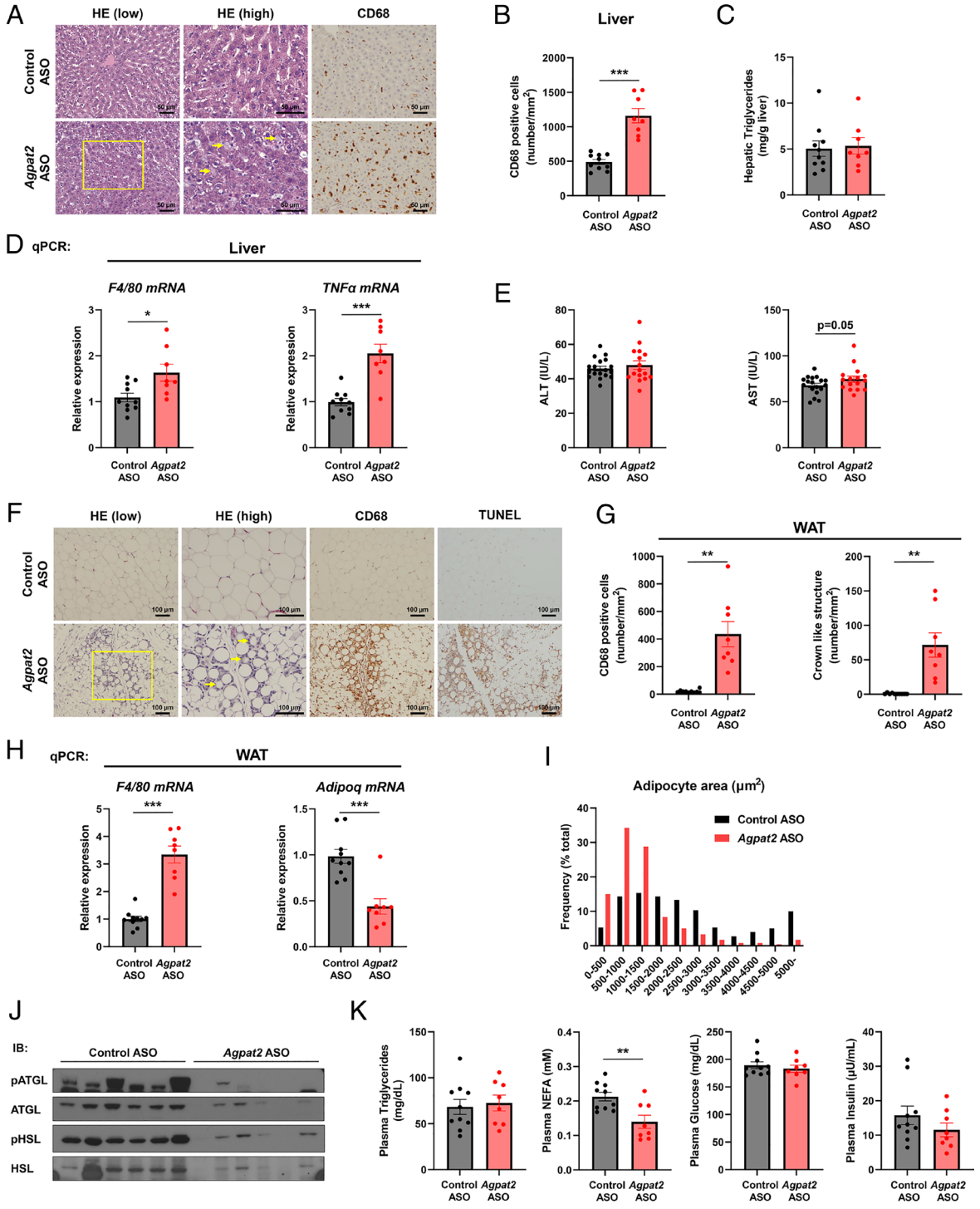

Fig. 2. *Agpat2* ASO induces inflammation in the liver and WAT and leads to loss of WAT. (*A*) Liver sections were stained with hematoxylin and eosin (HE), and CD68. The boxed area in HE (low) is magnified in HE (high). *Agpat2* ASO-treated rats showed liver lobule with increased macrophage infiltration (indicated by yellow arrows) confirmed with CD68 immunohistochemical stain. (*B*) Numbers of CD68-positive cells increased in *Agpat2* ASO-treated rats. Control ASO: $n = 10$, *Agpat2* ASO: $n = 8$. (*C*) Hepatic triglyceride content was not different between groups. Control ASO: $n = 10$, *Agpat2* ASO: $n = 8$. (*D*) RT-qPCR analysis demonstrated that hepatic mRNA expression of *F4/80* and *TNF-α* increased in *Agpat2* ASO-treated rats. Control ASO: $n = 10$, *Agpat2* ASO: $n = 8$. (*E*) Plasma ALT and AST levels. AST levels slightly increased in *Agpat2* ASO-treated rats. Control ASO: $n = 18$, *Agpat2* ASO: $n = 16$. (*F*) WAT sections were stained with HE, CD68, and terminal deoxynucleotidyl transferase dUTP nick end labeling (TUNEL) staining. The boxed area in HE (low) is magnified in HE (high). *Agpat2* ASO-treated rats showed crown-like structures (indicated by yellow arrows). Accordingly, CD68-positive cells increased in *Agpat2* ASO-treated rats. TUNEL-positive cells were undetectable in WAT of control ASO-treated rats. In contrast, TUNEL-positive cells were abundant in the *Agpat2* ASO-treated rats. (*G*) Numbers of CD68-positive cells and crown-like structures in WAT increased in *Agpat2* ASO-treated rats. Control ASO: $n = 10$, *Agpat2* ASO: $n = 8$. (*H*) RT-qPCR analysis of mRNA expression in WAT. *F4/80* mRNA increased, and *Adipoq* mRNA decreased in *Agpat2* ASO-treated rats, respectively. Control ASO: $n = 10$, *Agpat2* ASO: $n = 8$. (*I*) A histogram of adipocyte size distribution demonstrated that most adipocytes were smaller in *Agpat2* ASO-treated rats. Each plot represents a distribution of an individual adipocyte population according to size (area). Each distribution was obtained from 10 control ASO-treated rats and 8 *Agpat2* ASO-treated rats. (*J*) ATGL and HSL protein expression was analyzed in WAT by immunoblot analysis. *Agpat2* ASO-treated rats intensively decreased ATGL and HSL protein expression in WAT. Control ASO: $n = 6$, *Agpat2* ASO: $n = 6$. Vertically stacked strips of bands were evaluated in the same experimental conditions of Fig. 1*C*. (*K*) Plasma triglyceride and NEFA concentrations. Plasma NEFA decreased in *Agpat2* ASO-treated rats. Plasma insulin levels did not change. Control ASO: $n = 10$, *Agpat2* ASO: $n = 8$ The data are shown as the mean ± SEM. $*P < 0.05$; $**P < 0.01$; and $***P < 0.001$ (Student *t* test).

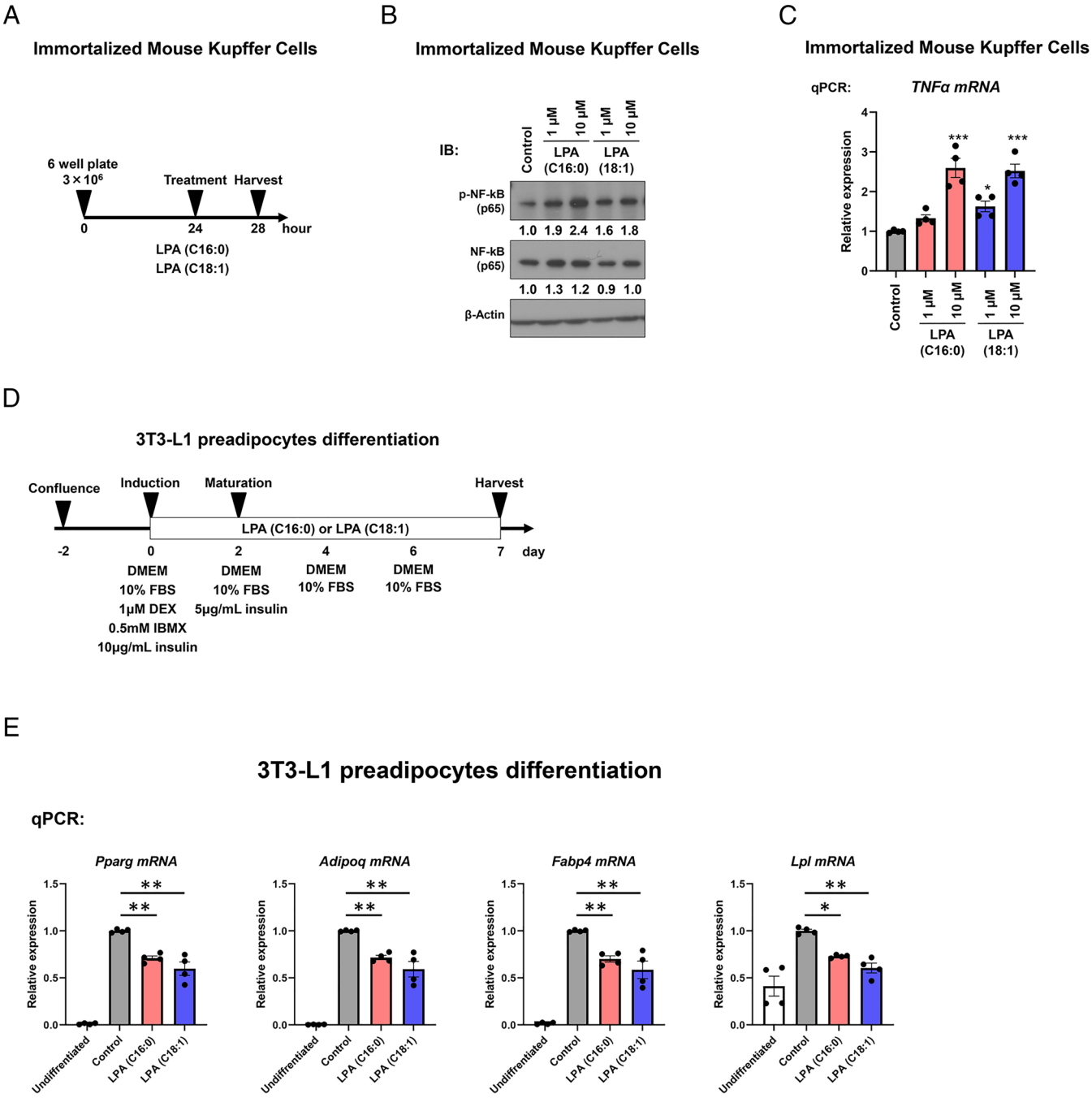

Fig. 3. LPA induces *TNFα* expression in Immortalized Mouse Kupffer Cells and suppresses adipocyte differentiation in 3T3-L1 cells. (*A*) Schematic diagram of the Immortalized Mouse Kupffer Cells study. Immortalized Mouse Kupffer Cells were plated on 6-well plate (3×10^6 cells/well) and then treated with palmitoyl LPA (C16:0) 1 or 10 μM or oleoyl LPA (C18:1) 1 or 10 μM for 4 h. (*B*) Representative immunoblot analysis of phosphorylated NF-kB/ total NF-kB in ImKC cells treated with Control, LPA 16:0 and LPA 18:1. β-actin was used as a loading control. NF-kB (p65) phosphorylation increased upon exposure to LPA (C16:0) or LPA (C18:1). (*C*) mRNA expression levels of *TNFα* by RT-qPCR in LPA-treated ImKC cells. Stimulation of ImKC cells with LPA significantly induced *TNFα* mRNA levels. Control: $n = 4$, LPA(C16:0) 1 μM: $n = 4$, LPA(C16:0) 10 μM: $n = 4$, LPA(C18:1) 1 μM: $n = 4$, LPA(C18:1) 10 μM: $n = 4$ The data are presented as the mean ± SEM. $^*P < 0.05$; $^{**}P < 0.01$, and $^{***}P < 0.001$ vs. control (one-way ANOVA test followed by Dunnett's multiple comparison test). (*D*) Schematic diagram of a procedure on 3T3-L1 preadipocyte differentiation. Two-day postconfluent 3T3-L1 cells were subjected to adipocyte differentiation for 7 d. For adipogenic differentiation, cells were placed in an induction medium consisting of Dulbecco's Modified Eagle Medium (DMEM), 10% fetal bovine serum (FBS), 0.5 mM 3-isobutyl-1-methylxanthine (IBMX), 1 μM dexamethasone (DEX), and 10 μg/mL insulin. After 48 h, the medium was switched to a maturation medium composed of DMEM, 10% FBS, and 5 μg/mL insulin. The medium was replenished every other day. Palmitoyl LPA (C16:0) and oleoyl LPA (C18:1) were added at concentrations of 10 μM, respectively, every other day. (*E*) On the 7th day of 3T3-L1 preadipocyte differentiation, mRNA expression of *Pparg*, *Adipoq*, *Fabp4*, and *Lpl* decreased in LPA (C16:0)-treated and LPA (C18:1)-treated 3T3-L1 cells compared to differentiated control. Undifferentiated: $n = 4$, control: $n = 4$, LPA (C16:0) $n = 4$, LPA (C18:1) 1 μM: $n = 4$. The data are presented as the mean ± SEM. $^*P < 0.05$; $^{**}P < 0.01$, and $^{***}P < 0.001$ vs. control (one-way ANOVA test followed by Dunnett's multiple comparison test)

and individual PA species showed no differences (Fig. 5*C*). WAT total LPA and PA content and all individual LPA species were not different between groups (Fig. 5*D*) except for the PA species (C16:0, C18:2) (Fig. 5*E*).

In the liver, *Gpam* ASO treatment resulted in decreased macrophage infiltration and CD68-positive cells (Fig. 5 *F* and *G*) and led to a reduction in hepatic triglyceride content compared to the control rats (Fig. 5*H*). Consistent with these results, *Gpam* ASO

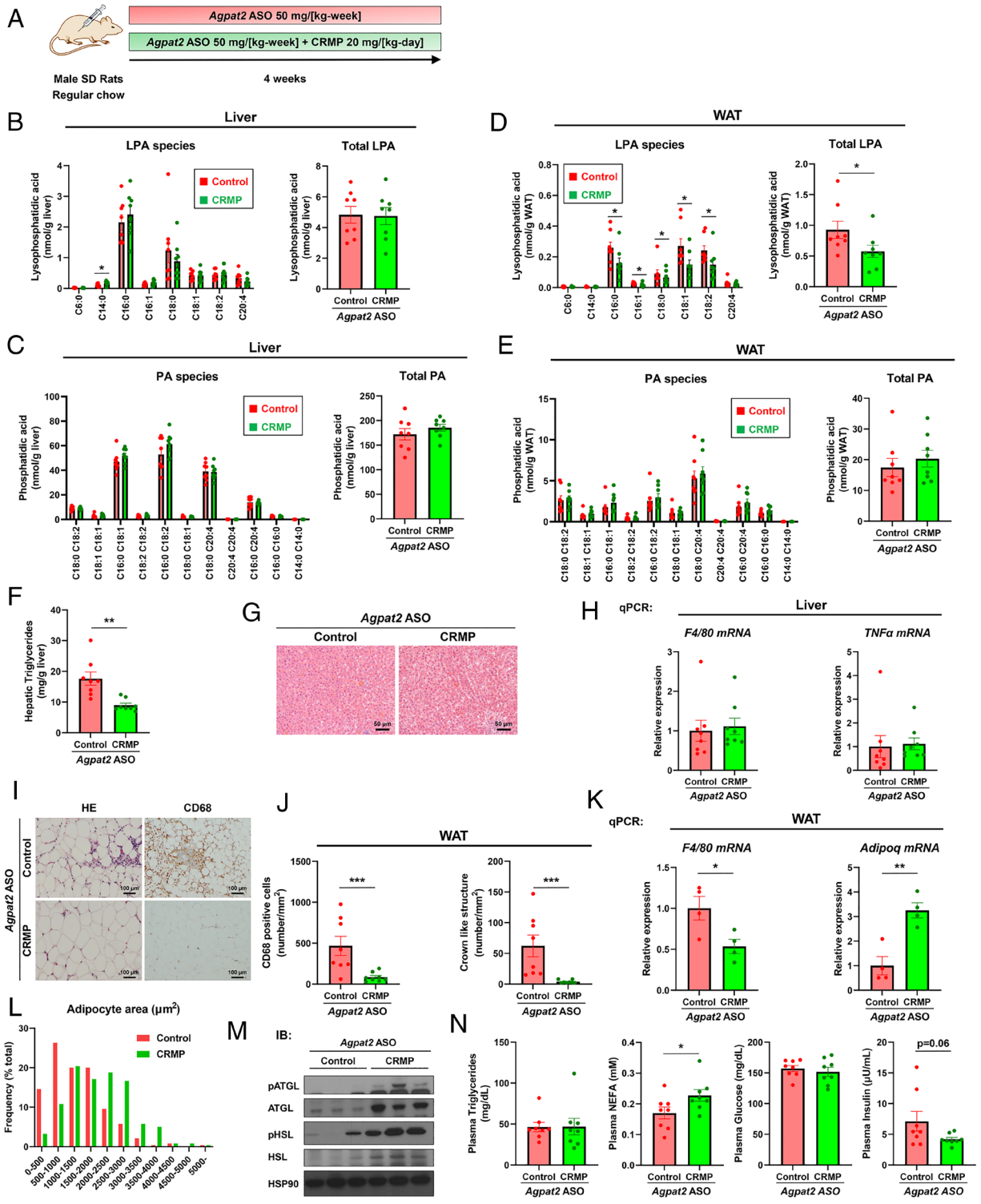

Fig. 4. Controlled-release mitochondrial protonophore treatment prevents LPA accumulation and inflammation in WATs in AGPAT2 deficiency. (*A*) Male SD rats were fed regular chow and treated with 50 mg/kg/week *Agpat2* ASO with or without controlled-release mitochondrial protonophore (CRMP) for 4 wk. (*B–E*) LPA and PA were extracted from livers and WATs and measured by tandem mass spectrometry. (control $n = 8$, CRMP $n = 8$). (*B*) The total hepatic LPA content showed no difference except for LPA (C14:0). (*C*) Total hepatic PA content and all individual PA species showed no differences. (*D*) The total WAT LPA content was decreased in CRMP-treated rats. Especially, LPA (C16:0), LPA (C16:1), LPA (C18:0), LPA (C18:1), and LPA (C18:2) decreased. (*E*) Total WAT PA content and all individual PA species showed no differences. (*F*) Hepatic triglyceride content decreased in CRMP-treated rats. Control: $n = 8$, CRMP: $n = 8$. (*G*) Liver sections were stained with HE. Control and CRMP-treated rats showed similar degree of inflammatory cell infiltration in the liver. (*H*) RT-qPCR analysis demonstrated that hepatic mRNA expression of *F4/80* and *TNF-α* showed no differences. Control: $n = 8$, CRMP: $n = 8$. (*I*) WAT sections were stained with HE and CD68. CD68-positive cells decreased in CRMP-treated rats. (*J*) CD68-positive cells and crown-like structures in WAT decreased in CRMP-treated rats. Control: $n = 8$, CRMP: $n = 8$. (*K*) RT-qPCR analysis of mRNA expression in WAT. *F4/80* mRNA decreased, and *Adipoq* mRNA increased in CRMP-treated rats, respectively. Control: $n = 4$, CRMP: $n = 4$. (*L*) A histogram of adipocyte size distribution demonstrated that most adipocytes were bigger in CRMP-treated rats. Each plot represents a distribution of an individual adipocyte population according to size (area). Each distribution was obtained from 8 control rats and 8 CRMP-treated rats. (*M*) ATGL and HSL protein expression was analyzed in WAT by immunoblot analysis. CRMP-treated rats increased ATGL and HSL protein expression in WAT. Control: $n = 3$, CRMP: $n = 3$. (*N*) Plasma triglyceride and Non-Esterified Fatty Acids (NEFA) concentrations. Plasma NEFA increased in CRMP-treated rats. Plasma insulin levels decreased in CRMP-treated rats. Control: $n = 8$, CRMP: $n = 8$ The data are shown as the mean ± SEM. $^*P < 0.05$; $^{**}P < 0.01$; and $^{***}P < 0.001$ (Student *t* test).

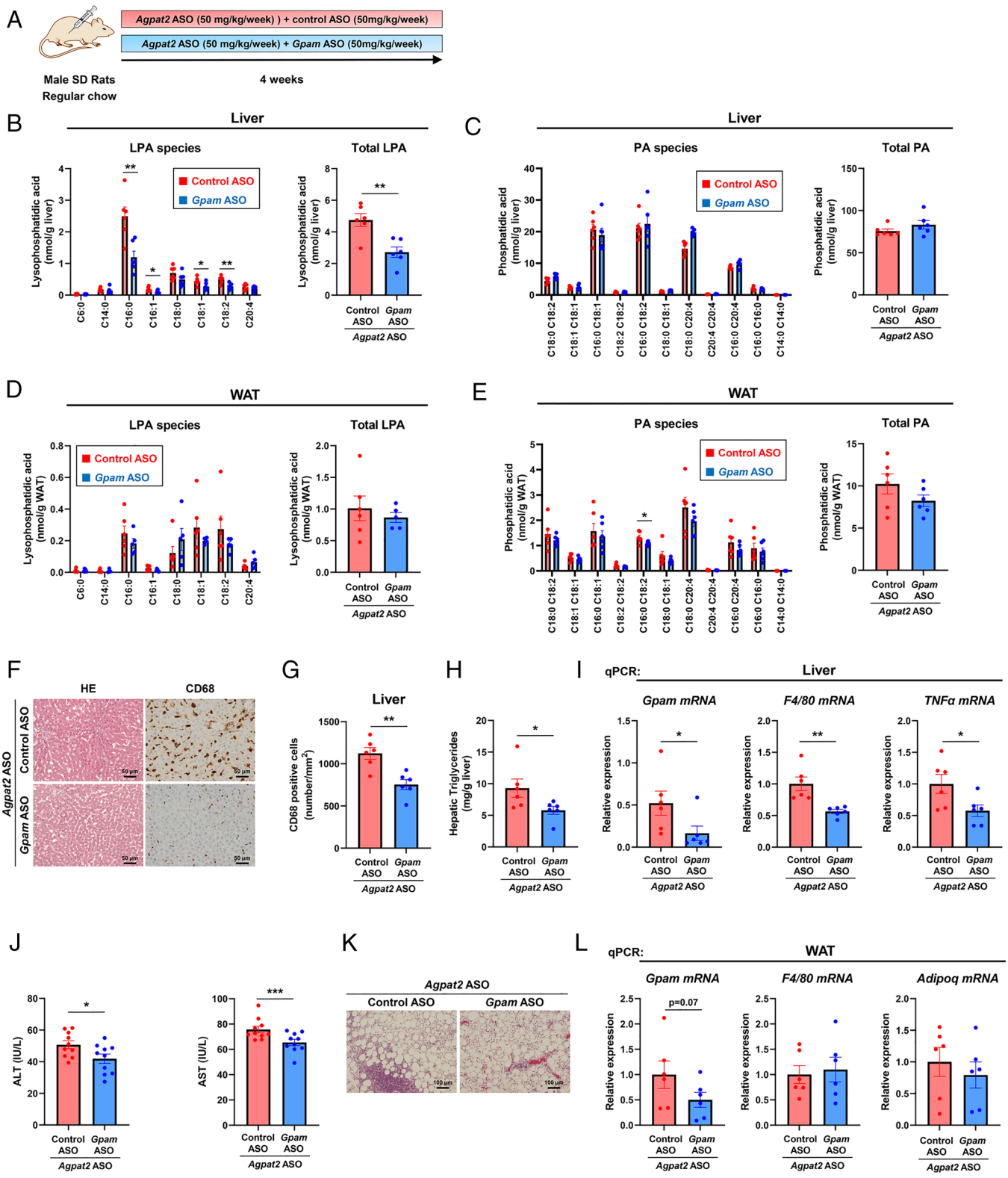

Fig. 5. *Gpam* ASO prevents hepatic LPA accumulation and inflammation in AGPAT2 deficiency. (*A*) Male SD rats were fed regular chow and treated with 50 mg/kg/week *Agpat2* ASO and control ASO or 50 mg/kg/week *Agpat2* ASO and *Gpam* ASO for 4 wk. (*B–E*) LPA and PA were extracted from livers and WAT and measured by tandem mass spectrometry. (control ASO $n = 6$, *Gpam* ASO $n = 5–6$). (*B*) The total hepatic LPA content was decreased in *Gpam* ASO-treated rats. Especially, LPA (C16:0), LPA (C16:1), LPA (C18:1), and LPA (C18:2) decreased. (*C*) Total hepatic PA content and all individual PA species showed no differences. (*D*) The total WAT LPA content and all individual LPA species showed no difference. (*E*) Total WAT PA content and all individual PA species showed no differences except for PA (C16:0, C18:2). (*F*) Liver sections were stained with HE, and CD68. CD68-positive cells decreased in *Gpam* ASO-treated rats. (*G*) CD68-positive cells in the liver decreased in *Gpam* ASO-treated rats. Control ASO: $n = 6$, *Gpam* ASO: $n = 6$. (*H*) Hepatic triglyceride content decreased in *Gpam* ASO-treated rats. Control ASO: $n = 6$, *Gpam* ASO: $n = 6$. (*I*) RT-qPCR analysis demonstrated that hepatic mRNA expression of *F4/80* and *TNFα* decreased in *Gpam*-ASO-treated rats. *Gpam* ASO decreased *Gpam* mRNA expression. Control ASO: $n = 6$, *Gpam* ASO: $n = 6$. (*J*) Plasma ALT and AST levels decreased in *Gpam*-ASO-treated rats. Control ASO: $n = 10$, *Gpam* ASO: $n = 10$. (*K*) WAT sections were stained with HE. Control ASO and *Gpam* ASO-treated rats showed similar degree of inflammatory cell infiltration in WAT. (*L*) RT-qPCR analysis demonstrated no differences in WAT mRNA expression of *F4/80* and *Adipoq*. *Gpam* ASO decreased *Gpam* mRNA expression. Control ASO: $n = 6$, *Gpam* ASO: $n = 6$. The data are shown as the mean ± SEM. $^*P < 0.05$; $^{**}P < 0.01$; and $^{***}P < 0.001$ (Student *t* test).

treatment also resulted in reductions in hepatic *F4/80* and *TNFα* mRNA expression (Fig. 5*I*) and plasma ALT and AST levels compared to the control group (Fig. 5*J*). In contrast to these effects in the liver and consistent with the lack of change in WAT LPA content, *Gpam* ASO treatment did not affect inflammation in WAT (Fig. 5 *K* and *L*).

Hepatic De Novo Lipogenesis Contributes to Hepatic LPA Content. The predominance of palmitoyl LPA (C16:0) content (Fig. 1*E*) in *Agpat2* ASO-treated rats fed a regular chow (i.e., low-fat) diet suggests that hepatic LPA arises from increased hepatic de novo lipogenesis. To examine whether hepatic LPA might be generated by hepatic de novo lipogenesis, we first assessed the impact of one week high-sucrose diet feeding on de novo lipogenesis using D_2O, which would be expected to further promote increased hepatic de novo lipogenesis, compared to a regular chow diet (Fig. 6*A*). As expected, hepatic de novo lipogenesis and hepatic triglyceride content increased further in high sucrose diet-treated rats compared to regular chow-treated rats (Fig. 6*B*). The total hepatic LPA content was increased in high sucrose diet-treated rats (Fig. 6*C*). While multiple species were increased by a high-sucrose diet, C16:0 LPA remained the major LPA species. The relative rate of LPA derived from de novo lipogenesis increased in high sucrose diet-treated rats compared to regular chow-treated rats while plasma deuterium oxide enrichment was similar between regular chow-treated rats and high sucrose diet-treated rats (Fig. 6*D*). The total LPA content in WAT was unchanged by a high-sucrose diet (Fig. 6*E*). High sucrose diet-treated rats manifested hepatic steatosis (Fig. 6*F*) and increased content of CD68-positive cells compared to the regular chow fed rats (Fig. 6 Fand *G*).

Next, we investigated whether *Gpam* ASO treatment would reduce high sucrose diet-induced increases in hepatic LPA content and CD68-positive cells content in rats fed a high sucrose diet to test whether decreasing hepatic LPA using *Gpam* ASO would alleviate liver inflammation in this rat model of overnutrition (Fig. 6*H*). Consistent with this hypothesis, total LPA content in the liver decreased in *Gpam* ASO-treated rats compared to control ASO-treated rats (Fig. 6*I*). *Gpam* ASO treatment also alleviated high sucrose diet-induced steatosis and resulted in decreased CD68-positive cells compared to the control rats (Fig. 6 *J* and *K*).

Discussion

In this study, we investigated the impact of AGPAT2 deficiency on liver and WAT LPA content and inflammation. We found that knockdown of Agpat2 in the liver and WAT, using an ASO, led to accumulation of LPA in the liver and WAT, which was associated with lipodystrophy and inflammation in these tissues. These results are consistent with a previous report of an *Agpat2* knockout mouse model which developed lipodystrophy and adipose inflammation, although LPA concentrations in WAT were not measured in this study (4). Knockdown efficacy of *Agpat2* ASO in our study was 60% in the liver and 40% in WAT, respectively (Fig. 1 *A*–*C*). While there are no studies addressing the phenotype of heterozygous *Agpat2* knockout mice, there is good reason to believe that partial knockdown of AGPAT2 should cause a phenotype. For example, recently AGPAT2 knockdown, using antisense RNA, in fish was shown to cause abnormal liver tissue structure resulting in liver damage (20).

Although PA is the product of AGPAT2, total hepatic PA content showed no differences (Fig. 1*G*). This result is consistent with prior AGPAT2 deficiency studies demonstrating compensatory increases in phospholipase D activity and diacylglycerol kinase activity leading to increased hydrolysis of phosphatidylcholine to PA and increased phosphorylation of diacylglycerol to PA respectively (5). Recently AGPAT2 deficiency has also been shown to compromise the stability of CDP-diacylglycerol synthases (CDSs), leading to PA accumulation (7). As a result, AGPAT2 deficiency is known not to decrease the level of its product, PA.

LPA signals through its G-protein coupled receptors (LPAR1-6) which exhibit widespread but differential cell and tissue distribution. The length of the fatty acid chain and the degree of unsaturation of fatty acids determine the receptor selectivity and physiological effects of LPA. Oleoyl LPA (C18:1) possesses high affinity for all isoforms of LPA receptors (21). Regarding inflammation/immune cell activation, LPA regulates GPCR signaling and IKK-NF-κB activation (11). LPA-mediated GPR35 signaling in intestinal macrophages results in TNFα production associated with NF-kB activation (12). Kupffer cells express *Lpar1-6* mRNAs (22). In this study, LPA treatment activated NF-kB and *TNFα* expression in ImKC cells (Fig. 3 *A-C*). *TNFα* is a well-described proinflammatory cytokine that causes liver inflammation (23). LPA was shown to have excellent permeability in a parallel artificial membrane permeability assay (24). This raises the possibility that intracellular LPA could be released from the hepatocytes and subsequently contribute to the pathogenesis of liver injury via LPA receptor-dependent signaling in surrounding cells. Based on our findings in the ImKC cell study and the previous results, it is possible that accumulated hepatic intracellular LPA in *Agpat2* ASO-treated rats would be released from hepatocytes to diffuse outside and bind to LPA receptors of Kupffer cells leading to increased *TNFα* expression.

Newborn *Agpat2* knockout mice have normal white and brown adipose tissue mass and loss of both of these adipose tissue depots occur during the first week of life (4). In contrast, human congenital generalized lipodystrophy (CGL), due to AGPAT2 deficiency, typically demonstrates near total absence of body fat at birth or soon after that (25). No direct evidence addresses the loss of adipose tissues during the perinatal period in human CGL1 patients due to *AGPAT2* mutations. Some case reports regarding human CGL1 infants due to *AGPAT2* mutations described no remarkable change at birth (26–28). Generalized loss of adipose was noted at 2 mo, 4.5 mo, or 7 y, respectively, in these case reports. Considering these findings, loss of adipose tissues during the prenatal period or shortly after birth may be expected to play a role in human CGL1 pathogenesis, similar to the *Agpat2* knockout mice.

Previous studies have suggested that AGPAT2 deficiency causes lipodystrophy via impaired triglyceride synthesis in adipocytes, suppressed adipocyte differentiation and function due to alterations in phospholipid synthesis (25) as well as postnatal adipocyte death resulting in acute local inflammation (4). A previous report showed that LPA decreased PPARγ expression and reduced adipocyte mRNA marker expressions during 3T3-F442A adipocyte differentiation and the inhibitory effect of LPA on adipocyte differentiation was not observed in the LPA1 receptor knockout primary preadipocyte (15). Consistent with these findings, LPA treatment decreased *Pparg* and its target genes mRNA expression in 3T3-L1 preadipocyte differentiation (Fig. 3 *D* and *E*). Our findings, in combination with the prior in vitro investigations, support a role for LPA-mediated suppression of adipocyte differentiation in the development of lipodystrophy due to AGPAT2 deficiency.

A previous *Agpat2* knockout mouse study demonstrated that both increased inflammation markers and apoptosis markers (TUNEL-positive cells) were found in adipose tissue at P0.5 (4). Consistent with these results, we confirmed TUNEL-positive cells with inflammation in WAT of *Agpat2* ASO-treated rats (Fig. 2*F*).

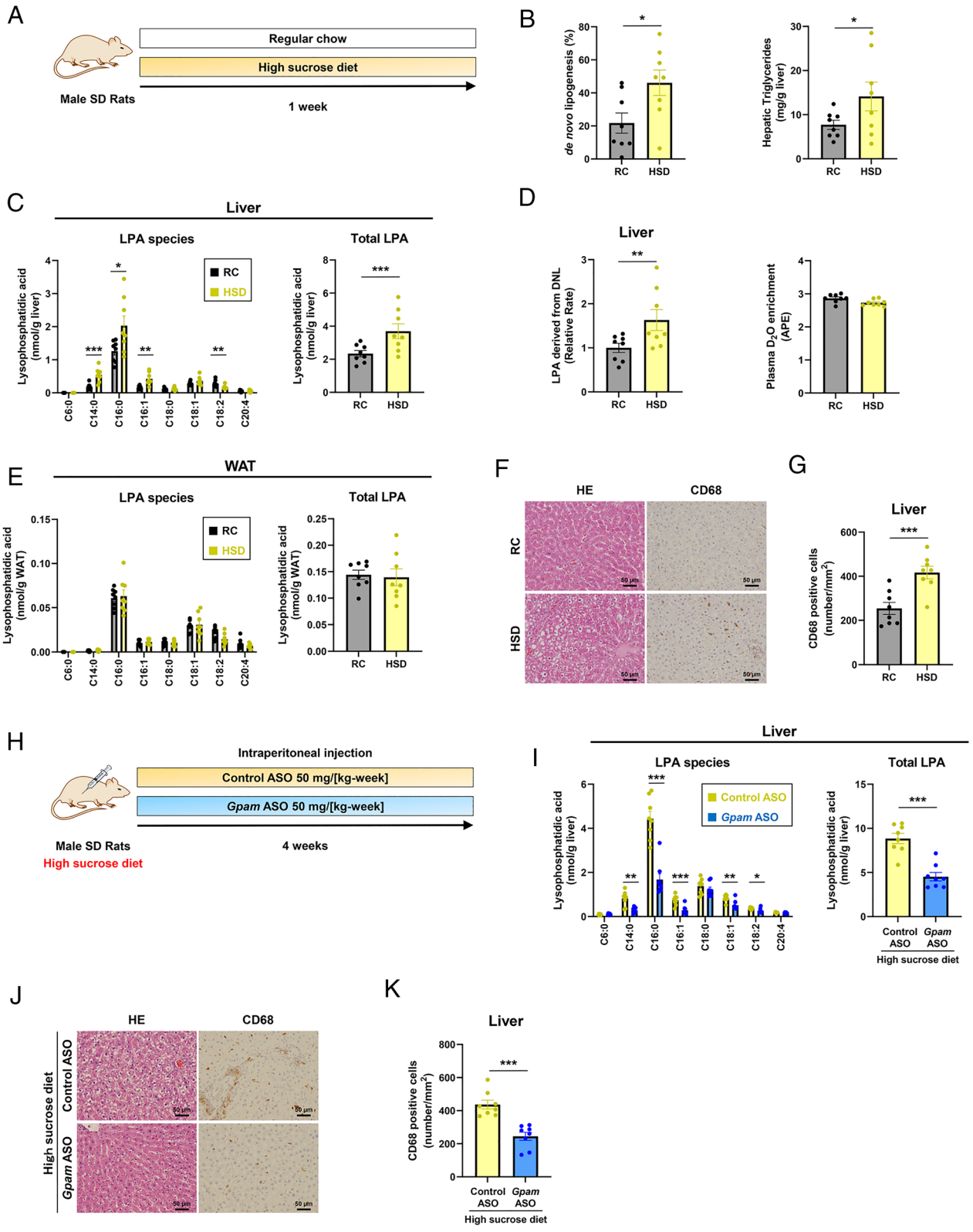

Fig. 6. High sucrose feeding induces increased hepatic de novo lipogenesis, which promotes increased hepatic LPA content and inflammation, which are both abrogated with *Gpam* ASO treatment. (A–G) Male SD rats were fed regular chow or high sucrose diet for 1 wk. (*B*) De novo hepatic lipogenesis and hepatic triglyceride content increased in high sucrose diet (HSD)-treated rats compared to regular chow (RC)-treated rats. RC: $n = 8$, HSD: $n = 8$. (*C*) The total hepatic LPA content was increased in HSD-treated rats. Most abundant LPA species in the liver were palmitoyl LPA (C16:0). RC: $n = 8$, HSD: $n = 8$. (*D*) The relative rates of LPA derived from de novo lipogenesis (DNL) increased in HSD-treated rats compared to RC-treated rats. Plasma deuterium oxide (D_2O) enrichment was similar between RC-treated rats and HSD-treated rats. RC: $n = 8$, HSD: $n = 8$. (*E*) The total LPA content in WAT was unchanged. RC: $n = 8$, HSD: $n = 8$. (*F*) Liver sections were stained with HE, and CD68. HSD treated rats showed steatosis and increased CD68-positive cells. (*G*) Numbers of CD68-positive cells increased in HSD-treated rats. RC: $n = 8$, HSD: $n = 8$. (*H–K*) Male SD rats were treated with 50 mg/kg/week control ASO of *Gpam* ASO for 4 wk during high sucrose diet feeding. (*I*) The total hepatic LPA content was decreased in *Gpam* ASO-treated rats. Especially, LPA (C14:0), LPA (C16:0), LPA (C16:1), LPA (C18:1), and LPA (C18:2) decreased. (*J*) Liver sections were stained with HE and CD68. CD68-positive cells decreased in *Gpam* ASO-treated rats. (*K*) CD68-positive cells in the liver decreased in *Gpam* ASO-treated rats. Control ASO: $n = 8$, *Gpam* ASO: $n = 8$. The data are shown as the mean ± SEM. $^*P < 0.05$; $^{**}P < 0.01$; and $^{***}P < 0.001$ (Student *t* test).

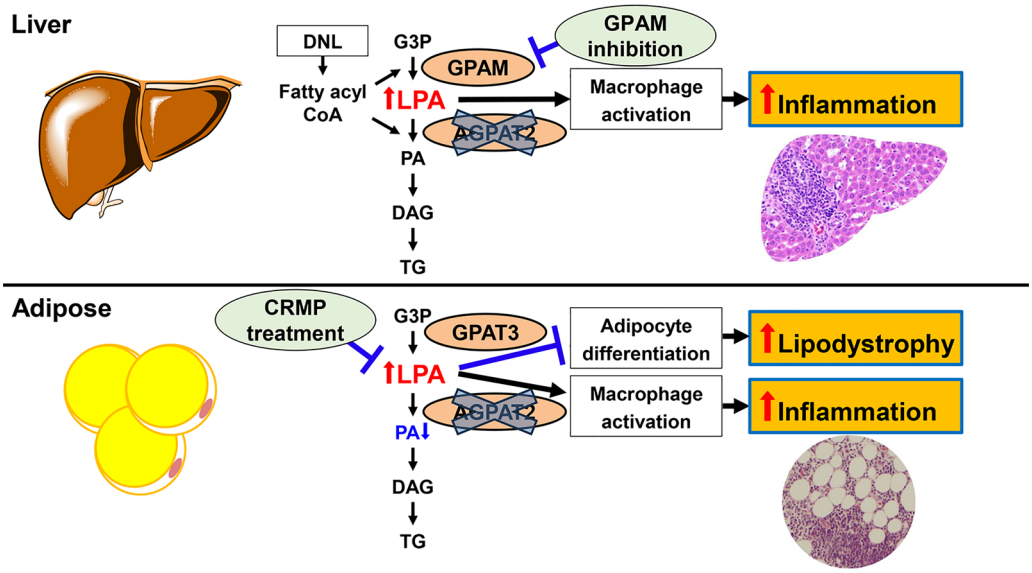

Fig. 7. The role of LPA on AGPAT2 deficiency. AGPAT2 deficiency increases LPA in the liver and WAT. LPA causes inflammation in the liver and WAT in addition to lipodystrophy. Controlled-release mitochondrial protonophore (CRMP) treatment primarily prevents LPA accumulation and inflammation in WAT and lipodystrophy. In contrast, inhibition of glycerol-3-phosphate acyltransferase, mitochondrial (GPAM) primarily in the liver prevents LPA accumulation and inflammation in the liver. DNL, de novo lipogenesis; G3P, glycerol-3-phosphate; PA, phosphatidic acid; DAG, diacylglycerol; TG, triglyceride

Taken together our findings suggest that accumulation of LPA in WAT suppresses adipocyte differentiation and induces WAT inflammation in association with cell death, leading to lipodystrophy. Whether WAT inflammation precedes WAT death or WAT death precedes WAT inflammation in AGPAT2 deficiency requires further investigation.

In order to demonstrate a causal role for LPA in mediating liver and WAT inflammation, we used two treatments to decrease tissue LPA concentrations: mitochondrial uncoupling with CRMP and blockade of the biosynthesis of LPA with *Gpam* ASO. Serendipitously, these two treatments had distinct and tissue-specific decreases in LPA concentrations, which tracked with changes in tissue inflammation. While CRMP decreased LPA in WAT, *Gpam* ASO decreased LPA in the liver. Consistent with a critical role for LPA in the pathogenesis of the observed inflammation, we found that CRMP reduced inflammation in WAT and lipodystrophy in *Agpat2* ASO-treated rats (Fig. 4) and *Gpam* ASO decreased inflammation in the liver in *Agpat2* ASO-treated rats (Fig. 5).

GPATs are classified into four isoforms. GPAM (GPAT1) and GPAT2 are localized in the mitochondrial outer membrane. GPAT3 and GPAT4 are localized in the endoplasmic reticulum membrane. GPAM contributes to the synthesis of triglyceride, particularly in the liver. GPAM prefers saturated acyl-CoA, such as palmitoyl-CoA, and selectively transfers acyl-CoA to the sn-1 position of glycerol-3-phosphate. GPAT3 plays an essential role in triglyceride synthesis in WAT and shows catalytic activity toward a broad range of saturated and unsaturated long-chain fatty acyl-CoA. These findings support our observations that *Gpam* ASO reduced LPA levels in the liver, not in WAT, in *Agpat2* ASO-treated rats. The difference in LPA molecular species between the liver and WAT in this study is also consistent with the different preferences of GPAT in the liver and WAT and suggest that GPAT3 inhibition/knockdown may be a good candidate for reducing LPA in WAT and prevent WAT inflammation and lipodystrophy in AGPAT2 deficiency.

The predominance of palmitoyl LPA (C16:0) in the liver (Fig. 1*E*) suggests that hepatic de novo lipogenesis contributes to hepatic LPA content. Consistent with this hypothesis, we found that a lipogenic high sucrose diet increased both hepatic palmitoyl LPA and total LPA content (Fig. 6 *A*–*D*) and macrophage activation as reflected by CD-68 positive cells (Fig. 6 *F* and *G*). *Gpam* ASO treatment of sucrose-fed rats decreased liver LPA content and reduced CD-68 positive cells (Fig. 6 *H*–*K*). Taken together these results suggest that LPA may also be an early metabolic trigger for hepatic inflammation due to overnutrition, consistent with recent GWASs demonstrating that GPAM loss of function variants manifest a protective effect on the risk of metabolic-associated steatotic liver disease in humans (29–31).

In summary, AGPAT2 deficiency leads to LPA accumulation and inflammation in the liver and WAT. CRMP treatment prevents LPA accumulation and inflammation in WAT, whereas *Gpam* ASO treatment prevents hepatic LPA accumulation and inflammation in the liver in AGPAT2 deficiency. In addition, overnutrition due to high sucrose feeding results in increased hepatic LPA content and increased activated macrophage content, which are both abrogated with *Gpam* ASO treatment. Taken together, these data demonstrate that LPA triggers inflammation in the liver and WAT under conditions of AGPAT2 deficiency as well as liver inflammation under conditions of overnutrition and may be an excellent therapeutic target to ameliorate these conditions (Fig. 7).

Materials and Methods

Detailed descriptions of materials and methods are provided in *SI Appendix*, *Materials and Methods*. These describe animals, tissue lipid metabolites, plasma biochemical measurement, immunoblot analysis, quantitative reverse transcription PCR analysis, histological analysis, cell culture, and in vivo hepatic de novo lipogenesis studies.

Data, Materials, and Software Availability. All study data are included in the article and/or *SI Appendix*.

ACKNOWLEDGMENTS. We thank John Stack, Irina Smolgovsky, Dr. Yasuko Iwarkiri, the Yale Histology Core Service for their excellent technical assistance and Dr. Dean Yimlamai for his helpful discussions. This study was supported by grants from the NIH [R01 DK119968 (G.I.S.), R01 DK133143 (G.I.S.), P30 DK045735 (G.I.S.), R01 DK124272 (D.F.V.), R21 AA029457)]. I.S. was supported by the Manpei Suzuki Diabetes Foundation, Mishima Kaiun Memorial Foundation, and the Ministry of Education, Culture, Sports, Science and Technology (Japan) Fund for the

Promotion of Joint International Research (Fostering Joint International Research (A); #20KK0373).

Author affiliations: [a]Department of Internal Medicine, Yale School of Medicine, New Haven, CT 06520; [b]Department of Molecular Diagnosis, Graduate School of Medicine Chiba University, Chiba 260-8670, Japan; [c]Department of Pathology, Yale School of Medicine, New Haven, CT 06520; [d]Ionis Pharmaceuticals, Carlsbad, CA; [e]Department of Cellular and Molecular Physiology, Yale School of Medicine, New Haven, CT 06520; and [f]Howard Hughes Medical Institute, Chevy Chase, MD 20815

Author contributions: I.S. and G.I.S. designed research; I.S., R.C.G., P.K.L., M.K., D.Z., X.Z., and J.P.G. performed research; S.M. contributed new reagents/analytic tools; I.S., R.C.G., P.K.L., M.K., D.Z., X.Z., J.P.G., D.F.V., V.T.S., K.F.P., and G.I.S. analyzed data; and I.S., R.C.G., P.K.L., D.F.V., V.T.S., K.F.P., and G.I.S. wrote the paper.

Reviewers: R.J.B., NIH/NIDDK; and E.A.O., University of Michigan.

Competing interest statement: S.M. is an employee of Ionis Pharmaceuticals. G.I.S. consults for and has received research support from Ionis Pharmaceuticals; is a stockholder of Orsobio, which owns the Yale intellectual property for CRMP; is an inventor of the Yale patent for CRMP.

1. A. Karagiota, G. Chachami, E. Paraskeva, Lipid metabolism in cancer: The role of acylglycerolphosphate acyltransferases (AGPATs). *Cancers (Basel)* **14**, 228 (2022).
2. N. Patni, A. Garg, Congenital generalized lipodystrophies–New insights into metabolic dysfunction. *Nat. Rev. Endocrinol.* **11**, 522–534 (2015).
3. V. A. Cortes *et al.*, Molecular mechanisms of hepatic steatosis and insulin resistance in the AGPAT2-deficient mouse model of congenital generalized lipodystrophy. *Cell Metab.* **9**, 165–176 (2009).
4. K. M. Cautivo *et al.*, AGPAT2 is essential for postnatal development and maintenance of white and brown adipose tissue. *Mol. Metab.* **5**, 491–505 (2016).
5. S. Sankella, A. Garg, J. D. Horton, A. K. Agarwal, Hepatic gluconeogenesis is enhanced by phosphatidic acid which remains uninhibited by insulin in lipodystrophic Agpat2-/- mice. *J. Biol. Chem.* **289**, 4762–4777 (2014).
6. V. A. Cortés *et al.*, Leptin ameliorates insulin resistance and hepatic steatosis in Agpat2-/- lipodystrophic mice independent of hepatocyte leptin receptors. *J. Lipid Res.* **55**, 276–288 (2014).
7. H. Y. Mak *et al.*, AGPAT2 interaction with CDP-diacylglycerol synthases promotes the flux of fatty acids through the CDP-diacylglycerol pathway. *Nat. Commun.* **12**, 6877 (2021).
8. L. González-Hódar *et al.*, Decreased caveolae in AGPAT2 lacking adipocytes is independent of changes in cholesterol or sphingolipid levels: A whole cell and plasma membrane lipidomic analysis of adipogenesis. *Biochim. Biophys. Acta: Mol. Basis Dis.* **1867**, 166167 (2021).
9. P. J. Tapia *et al.*, Absence of AGPAT2 impairs brown adipogenesis, increases IFN stimulated gene expression and alters mitochondrial morphology. *Metab. Clin. Exp.* **111**, 154341 (2020).
10. E. Kaffe, C. Magkrioti, V. Aidinis, Deregulated lysophosphatidic acid metabolism and signaling in liver cancer. *Cancers (Basel)* **11**, 1626 (2019).
11. W. Sun, J. Yang, Molecular basis of lysophosphatidic acid-induced NF-κB activation. *Cell Signal* **22**, 1799–1803 (2010).
12. B. Kaya *et al.*, Lysophosphatidic acid-mediated GPR35 signaling in CX3CR1(+) macrophages regulates intestinal homeostasis. *Cell Rep.* **32**, 107979 (2020).
13. B. P. Gaire *et al.*, Lysophosphatidic acid receptor 5 contributes to imiquimod-induced psoriasis-like lesions through NLRP3 inflammasome activation in macrophages. *Cells* **9**, 1753 (2020).
14. J. Fransson *et al.*, Activation of macrophages by lysophosphatidic acid through the lysophosphatidic acid receptor 1 as a novel mechanism in multiple sclerosis pathogenesis. *Mol. Neurobiol.* **58**, 470–482 (2021).
15. M. F. Simon *et al.*, Lysophosphatidic acid inhibits adipocyte differentiation via lysophosphatidic acid 1 receptor-dependent down-regulation of peroxisome proliferator-activated receptor gamma2. *J. Biol. Chem.* **280**, 14656–14662 (2005).
16. B. Yang, Z. Zhou, X. Li, J. Niu, The effect of lysophosphatidic acid on Toll-like receptor 4 expression and the nuclear factor-κB signaling pathway in THP-1 cells. *Mol. Cell Biochem.* **422**, 41–49 (2016).
17. A. Abulizi *et al.*, A controlled-release mitochondrial protonophore reverses hypertriglyceridemia, nonalcoholic steatohepatitis, and diabetes in lipodystrophic mice. *FASEB J.* **31**, 2916–2924 (2017).
18. S. Neschen *et al.*, Prevention of hepatic steatosis and hepatic insulin resistance in mitochondrial acyl-CoA:glycerol-sn-3-phosphate acyltransferase 1 knockout mice. *Cell Metab.* **2**, 55–65 (2005).
19. K. Karasawa, K. Tanigawa, A. Harada, A. Yamashita, Transcriptional regulation of Acyl-CoA: Glycerol-sn-3-phosphate acyltransferases. *Int. J. Mol. Sci.* **20**, 964 (2019).
20. T. Feng *et al.*, Transcriptional inhibition of AGPAT2 induces abnormal lipid metabolism and oxidative stress in the liver of Nile Tilapia *Oreochromis niloticus*. *Antioxidants (Basel)* **12**, 700 (2023).
21. B. Meduri *et al.*, Lysophosphatidic acid (LPA) receptor modulators: Structural features and recent development. *Eur. J. Med. Chem.* **222**, 113574 (2021).
22. I. Lua, S. Balog, A. Yanagi, C. Tateno, K. Asahina, Loss of lysophosphatidic acid receptor 1 in hepatocytes reduces steatosis via down-regulation of CD36. *Prostaglandins Other Lipid Mediat.* **156**, 106577 (2021).
23. E. J. Park *et al.*, Dietary and genetic obesity promote liver inflammation and tumorigenesis by enhancing IL-6 and TNF expression. *Cell* **140**, 197–208 (2010).
24. M. Baader *et al.*, Characterization of the properties of a selective, orally bioavailable autotaxin inhibitor in preclinical models of advanced stages of liver fibrosis. *Br. J. Pharmacol.* **175**, 693–707 (2018).
25. A. K. Agarwal, A. Garg, Genetic disorders of adipose tissue development, differentiation, and death. *Annu. Rev. Genomics Hum. Genet.* **7**, 175–199 (2006).
26. P. Rostami *et al.*, AGPAT2 gene mutation in a child with Berardinelli-Seip congenital lipodystrophy syndrome. *Ann. Endocrinol. (Paris)* **74**, 59–61 (2013).
27. H. Chaudhary, I. Panigrihi, P. Bhatia, Oil Red-O Positive lipid blobs on peripheral blood film examination in a muscular infant with the diagnosis of Berardinelli–Seip syndrome. *Oxf. Med. Case Rep.*, omz062 (2019).
28. S. Costa *et al.*, Face-sparing congenital generalized lipodystrophy type 1 associated with nonclassical congenital adrenal hyperplasia. *J. Clin. Endocrinol. Metab.* **107**, 2433–2438 (2022).
29. G. Sveinbjornsson *et al.*, Multiomics study of nonalcoholic fatty liver disease. *Nat. Genet.* **54**, 1652–1663 (2022).
30. S. W. K. Ng *et al.*, Convergent somatic mutations in metabolism genes in chronic liver disease. *Nature* **598**, 473–478 (2021).
31. O. Jamialahmadi *et al.*, Exome-wide association study on alanine aminotransferase identifies sequence variants in the GPAM and APOE associated with fatty liver disease. *Gastroenterology* **160**, 1634–1646.e1637 (2021).